ISSN 1846-6168 (Print), ISSN 1848-5588 (Online)
https://doi.org/10.31803/tg-20240514145648

Original scientific paper
Received: 2024-05-14, Accepted: 2024-06-22

Development and Optimization of a Differential Signal-Based Fabry-Perot Interferometer for Nanopositioning

Syuan-Cheng Chang, Chung-Ping Chang*, Yung-Cheng Wang

Abstract: In this study, we present the optimization of a Fabry-Perot interferometer with a differential signal utilized as the laser encoder to meet the stringent demands of nanopositioning. The proposed system aims to enhance stability and accuracy in nanopositioning applications by leveraging the common path structure and coaxial characteristics of Fabry-Perot interferometers. To improve the resolution of this system, an interpolation module is employed to increase the laser encoder resolution to 15.82 nm. Compared to the simulated interference signal from traditional Fabry-Perot interferometers, the differential interference signal proposed in this study is more sinusoidal, thus reducing errors in resolution subdivision. To verify the correspondence between the actual interference signal and the simulated one, a signal testing experiment is implemented in this study. Eventually, the experimental signal results demonstrate that the actual light intensity signals match the simulated results, indicating that this signal can be significantly beneficial for use as a laser encoder.

Keywords: differential signal processing; Fabry-Perot interferometer; interpolation module; laser encoder; nanopositioning

1 INTRODUCTION

In recent years, nanotechnology has become a pivotal field with widespread implications across industries, driving the demand for precise and reliable nanopositioning techniques. Among these techniques, laser interferometry particularly as an encoder in nanopositioning systems plays a crucial role due to its ability to provide high-resolution and accurate measurements at the nanoscale. The integration of laser interferometry into nanopositioning technologies has greatly enhanced the capabilities and functionalities of nanopositioners, enabling precise manipulation and control of objects with exceptional precision and accuracy [1].

However, commercial interferometers such as the Michelson interferometers have been commonly used for linear positioning calibration, they are susceptible to disturbances between the measurement and reference arms [2]. According to recent research, Fabry-Perot interferometers offer outstanding measuring stability due to their common-path structure which minimizes the effects of disturbances in the reference arm. Therefore, in some novel research, the Fabry-Perot interferometer has also been applied in the displacement measuring system, yielding remarkable results [3]. In this study, we have improved upon previous research and continued the development of this measurement technique by optimizing interferometric systems based on Fabry-Perot interferometers for nanopositioning technologies [4-6].

This study focuses on developing an interferometric system based on this common path structure to eliminate DC offset, making it suitable for precise positioning control in normal environments. The goal is to provide wide-ranging positioning control applications in precision mechanical industries.

2 THEORY AND PRINCIPLE

In this chapter, a brief introduction to displacement Fabry-Perot interferometer technology is provided. Additionally, the design of the proposed differential Fabry-Perot interferometer is demonstrated as follows.

2.1 Conventional Fabry-Perot Interferometer

Fabry-Perot interferometer was invented by French physicists Charles Fabry and Alfred Perot in the late 19th century [7]. The optical structure of the well-known FPI is depicted in Fig. 1. The incident beam (I_0) travels forwards and backwards repeatedly, dividing into numerous transmitted beams which interfere with each other. The resulting fringe signals are acquired by the detector. The correlative equations of the intensity distribution can be described by Eq. (1), where R, d, and λ represent reflectance of the mirror, the length of the cavity, and the laser wavelength, respectively. Since the measurement and reference beams travel through the same environment, the displacement measured is precisely defined by the distance between two parallel mirrors [8]. Hence, such an optical structure is feasible for precision length measurement.

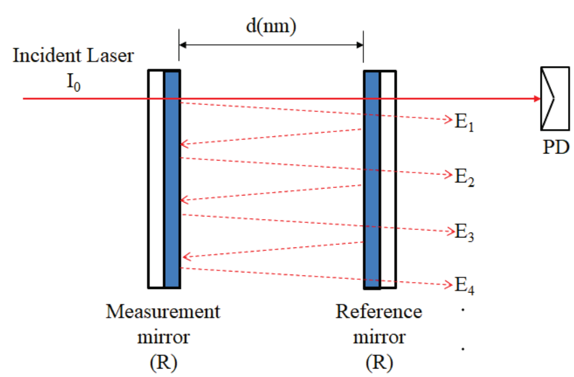

Figure 1 Conventional Fabry-Perot interferometer

$$I = I_0 \frac{(1-R)^2}{1+R^2 - 2\cdot R\cdot \cos\left(\frac{2\cdot\pi\cdot d}{\lambda\cdot\cos\alpha}\right)}. \quad (1)$$

Due to the conventional Fabry-Perot interferometer cannot determine the movement direction of the object. To address this limitation, a quadrature phase-shifted method based on polarizing technology has been proposed in previous research [9-11], as depicted in Fig. 2. In this polarizing phase-shifted method, a one-eighth waveplate is inserted into the optical cavity to generate quadrature phase-shifting. Consequently, the phase difference between the two interference signals is determined by the accuracy of the waveplate. The equations describing the intensity distribution of PD_s (I_s) and PD_P (I_P) are provided in Eq. (2) and (3).

The simulation result of the intensity distribution is shown in Fig. 3. Nevertheless, the signal offset of the polarizing phase-shifted method will be changed by the length of the cavity, the parallelism of the cavity, and the coherence of the laser source. It causes the interpolation error during the measurement procedure with the fine resolution.

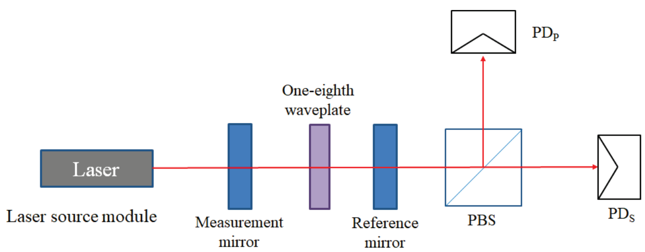

Figure 2 Quadrature phase-shift fiber FPI

$$I_s = E_s \cdot E_s^* = \frac{\frac{1}{2} \cdot A_0^2 \cdot T^2 \cdot T'}{1+R^2 \cdot T'^2 - 2 \cdot T' \cdot R \cdot \cos(2\delta)}, \quad (2)$$

$$I_p = E_p \cdot E_p^* = \frac{\frac{1}{2} \cdot A_0^2 \cdot T^2 \cdot T'}{1+R^2 \cdot T'^2 - 2 \cdot T' \cdot R \cdot \cos\left(2\delta + \frac{\pi}{2}\right)}. \quad (3)$$

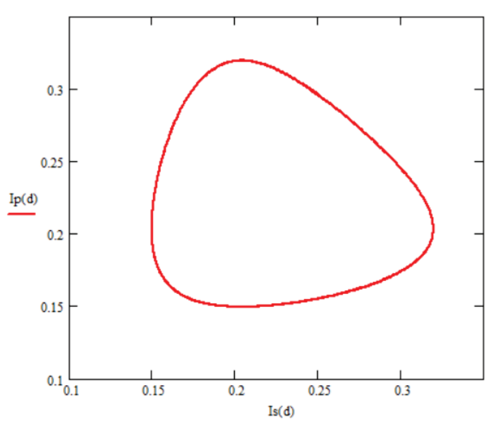

Figure 3 Intensity distribution of Quadrature phase-shift fiber FPI

2.2 Proposed Differential Fabry-Perot Interferometer

The optical structure of differential Fabry-Perot interferometer is shown in the Fig. 4. The incident laser passes through the optical cavity and the quarter-waveplate which is placed inside the cavity. The laser beams which include multiple right and left circular polarizing beams (E_1, E_2, E_3…) are divided into two circular polarizing beams by a beam splitter (BS). And each circular polarizing beam is divided into two multiple linear polarizing beams by a polarizing beam splitter (PBS). Those four interference signals can be detected by four photodetectors (PDs). The signals are divided by the same PBS and will have a phase shift of 180°. By rotating the half-waveplate, the phase shift of the interference signals can be adjusted into the proper position. Based on the previous research, the major purpose of the proposed structure can reduce the DC drift of the interference signal.

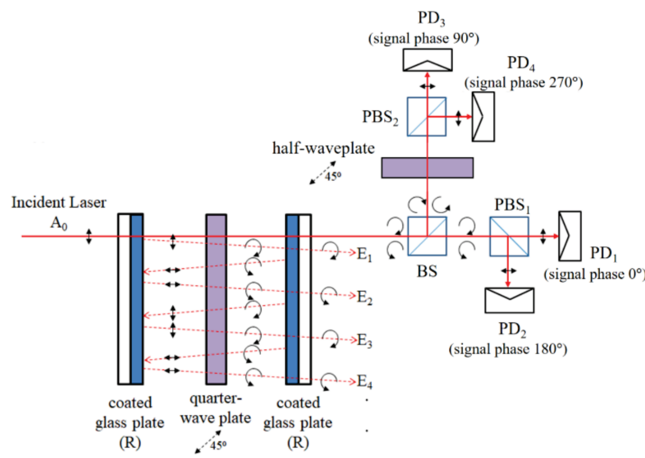

Figure 4 Differential Fabry-Perot interferometer

The equations of the transmitted electric field of the laser beams are expressed as E_1 to E_N (Eq. 4 to Eq. 7) and that of the whole interference beam is denoted with E_N (Eq. 7), where N is the order of the transmitted light beams. Here, $\boldsymbol{A}_0$, T, T_c, R, $\boldsymbol{WP}$, $OP(d)$ and $OPD(d)$ are the matrices and coefficients involved in the calculation of the electric field. $\boldsymbol{A}_0$ represents the matrix of the incident beam with linear polarization from the horizontal axis; T represents the transmittance of the coated glass plate; T_c represents the equivalent transmittance of the cavity; R represents the reflectance of the coated glass plate; WP represents the matrix of the quarter-waveplate with a 45-degree angle from the horizontal axis; $OP(d)$ represents the single-pass optical path within the optical cavity; $OPD(d)$ represents the optical path out of the optical cavity.

$$E_1 = \sqrt{T} \cdot \left(\sqrt{T_c} \cdot OPD(d) \cdot WP \cdot \sqrt{R}\right)^1 \cdot OP(d) \cdot \sqrt{T} \cdot \boldsymbol{A}_0, \quad (4)$$

$$E_2 = \sqrt{T} \cdot \left(\sqrt{T_c} \cdot OPD(d) \cdot WP \cdot \sqrt{R}\right)^3 \cdot OP(d) \cdot \sqrt{T} \cdot \boldsymbol{A}_0, \quad (5)$$

$$E_3 = \sqrt{T} \cdot \left(\sqrt{T_c} \cdot OPD(d) \cdot WP \cdot \sqrt{R}\right)^5 \cdot OP(d) \cdot \sqrt{T} \cdot \boldsymbol{A}_0, \quad (6)$$

$$E_N = \sqrt{T} \cdot \left(\sqrt{T_c} \cdot OPD(d) \cdot WP \cdot \sqrt{R}\right)^{2N-1} \cdot OP(d) \cdot \sqrt{T} \cdot \boldsymbol{A}_0. \quad (7)$$

In order to calculate the sum of the electric field (E_N), the odd term (E_{odd}) and the even term (E_{even}) of the electric field are separated for the calculation, as shown in Eq. (8) and (9).

$$E_N = E_{\text{odd}} + E_{\text{even}}, \tag{8}$$

$$E_N = = \left(E_1 + E_3 + E_5 + \ldots + E_{2N-1}\right) + \left(E_2 + E_4 + E_6 + \ldots + E_{2N}\right). \tag{9}$$

Eventually, the total electric field obtained by summing the odd term and even term of the electric field is shown in Eq. (10).

$$E_N = \left\{ \begin{bmatrix} \frac{1}{\sqrt{2}} \\ \frac{i}{\sqrt{2}} \end{bmatrix} \cdot T \cdot \mathrm{e}^{i(\omega t + kx)} \cdot \frac{\sqrt{T} \cdot \sqrt{R} \cdot \mathrm{e}^{i\frac{2\pi d}{\lambda}}}{1 - \left(\sqrt{T} \cdot \sqrt{R} \cdot \mathrm{e}^{i\frac{2\pi d}{\lambda}}\right)^4} \right\} + \left\{ \begin{bmatrix} \frac{-1}{\sqrt{2}} \\ \frac{i}{\sqrt{2}} \end{bmatrix} \cdot T \cdot \mathrm{e}^{i(\omega t + kx)} \cdot \frac{\left(\sqrt{T} \cdot \sqrt{R} \cdot \mathrm{e}^{i\frac{2\pi d}{\lambda}}\right)^3}{1 - \left(\sqrt{T} \cdot \sqrt{R} \cdot \mathrm{e}^{i\frac{2\pi d}{\lambda}}\right)^4} \right\}. \tag{10}$$

When E_N has been obtained, the intensity of 0°, 45°, 90°, and 135° of the polarizer axis can be acquired by Eq. (11).

$$I = E \cdot E^{*}. \tag{11}$$

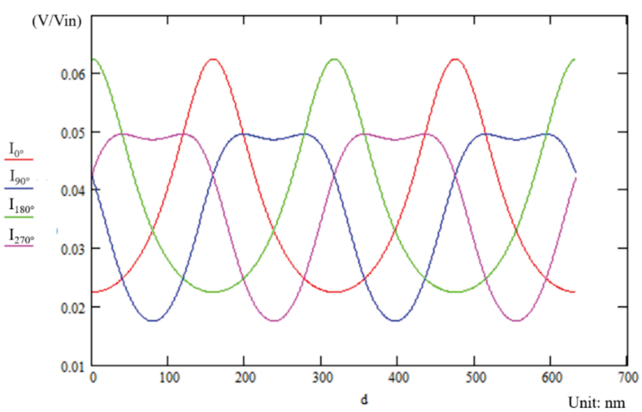

Figure 5 Simulation of the intensities in each phase

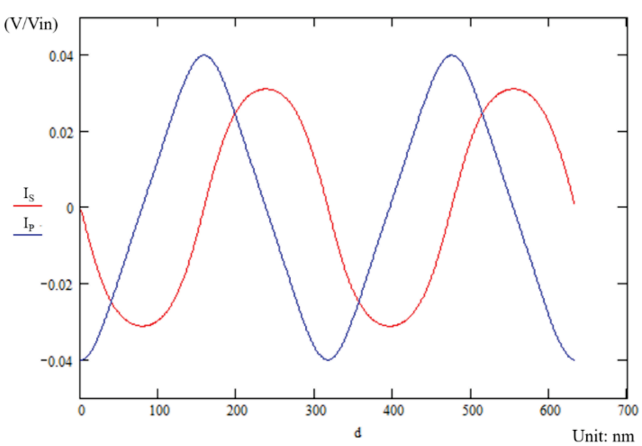

Figure 6 Simulation of differential signal

The simulation results of the intensity profiles for *I* (0°), *I* (45°), *I* (90°), and *I* (135°) are presented in Fig. 5. The processing principle of the differential signal involves subtracting one signal from the other, each having the same amplitude but opposite phase. Consequently, simulations of the differential signal and the Lissajous figure are depicted in Fig. 6 and Fig. 7(a), respectively. Comparing Fig. 7(a) and Fig. 7(b) can show that the simulation results of differential Fabry-Perot interferometer is a sinusoidal signal, whereas the simulation results of the QPSK FPI do not exhibit such sinusoidal signal.

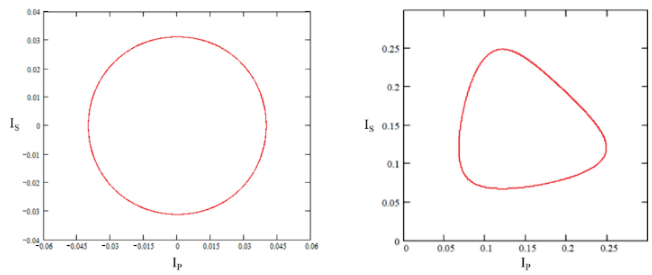

(a) R=25 %, T'= 87 % (b) R=25 %, T'= 87 %

Figure 7 Simulation of Lissajous figure (a) Simulation results of Differential FPI (b) Simulation results of QPSK FPI

3 DESIGN OF PROPOSED POSITIOINING SYSTEM

The positioning system proposed in this article utilizes the interference signal of the differetial Fabry-Pert interferometer as a laser encoder. This system consists of three main components: the light source unit (laser source and polarizer), the measurement unit (reference mirror, quarter-waveplate, and measurement mirror), and the sensing unit (BS, two PBS, half-waveplate, and four photodiodes), as illustrated in Fig. 8. Since the measurement mirror is installed on a linear stage, any displacement generated can be determined by oberving the amplitude of the light intensity received by the photodetecors (PD_1 to PD_4).

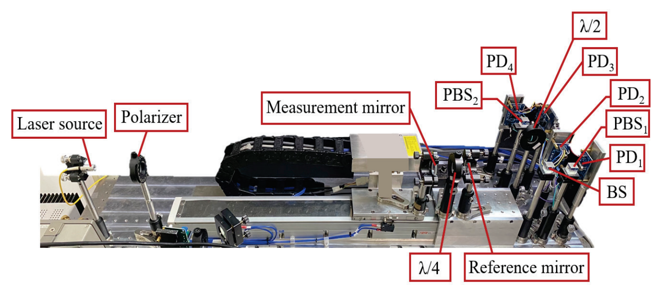

Figure 8 Design of proposed positioning system

The interpolation module is utilized in this study to convert the input orthogonal sine wave signal into a square wave signal. The resolution of the signal interpolation can be adjusted by modifying the circuit, and a interpolation reolusiton of 20 times is selected in this study. This means that within one sine wave cycle, five square waves are generated. Using the common fourfold frequency counting method in optical feedback signal processing, 20 counts can be obtained, as shown on Fig. 9. With an optical interference cycle of 316.4 nm, the positioning resolution can be deduced as 15.82 nm. The interpolation module can configure through external voltage to set the reference baseline of the signal. The specific procedure involves inputting the two orthogonal interference signals into the interpolation module. This yields the differential signal A+, A–, B+, B– which are utilized as the laser encoder to achieve the positioning objective.

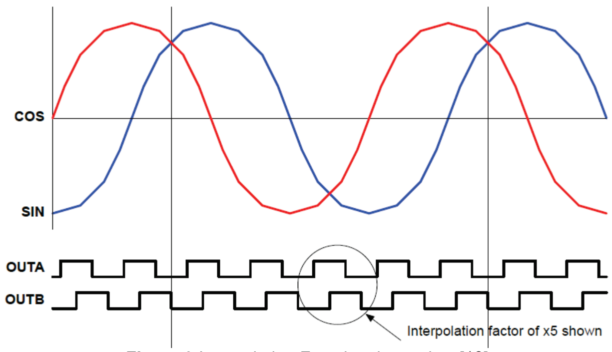

Figure 9 Interpolation Functional overview [12]

4 EXPERIMENTAL SIGNAL RESULTS

In order to verify the correspondence between the actual interference signal and the simulated one, experiments were conducted to measure the interference signal. According to the optical structure of the differential Fabry-Perot interferometer presented in Fig. 8, interference signal experiment was conducted. The light intensity signals detected by the photodetectors (PDs) are depicted in Fig. 9. It can be observed that the actual light intensity signals match the simulation shown in Fig. 5. The time-domain signal results from PD_1 to PD_4 are illustrated in Fig. 9(a) and 9(b), respectively.

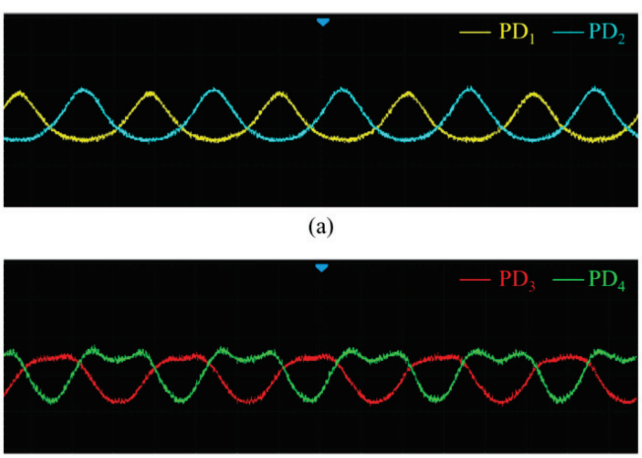

Figure 10 Interference signal from PD_1 to PD_4
(a) time-domain signal of PD_1 and PD_2, (b) time-domain signal of PD_3 and PD_4

By utilizing the principle of differential signal processing, the signals from PD_1 to PD_4 are subtracted to obtain the differential interference signal as shown in Figure 11. The light intensity signals from PD_1 and PD_2, with a phase difference of 180 degrees, are subtracted to obtain the sin signal. Similarly, subtracting the signals from PD_3 and PD_4, also with a phase difference of 180 degrees, yields the cos signal. The Lissajous figure can be represented by Fig. 12. These signals can represent the sinusoidal signal generated by the displacement of the linear stage.

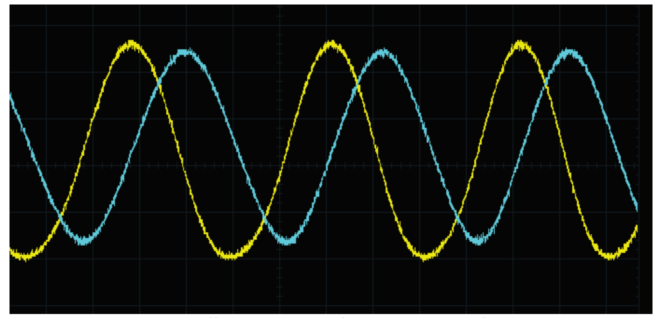

Figure 11 Differential signal of Fabry-Perot interferometer

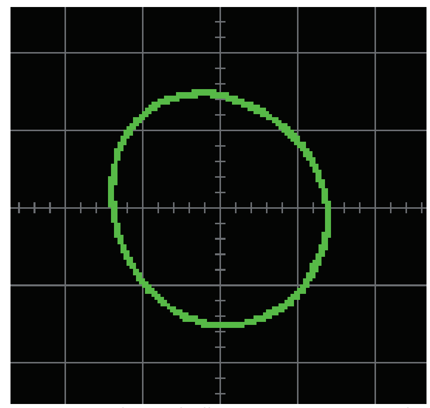

Figure 12 Lissajous figure of differential Fabry-Perot interferometer

After obtaining the differential signal through the principle of differential processing, signal processing can be conducted using the interpolation module proposed in this study. The differential signal is subjected to analog-to-digital conversion and further subdivided based on the selected subdivision ratio through this module. In this study, the resolution is subdivided by a factor of 20, thereby enhancing the resolution to 15.82 nm. If higher specifications are required, further subdivision can be performed according to the needs. The resulting signal after conversion can be represented by Fig. 13.

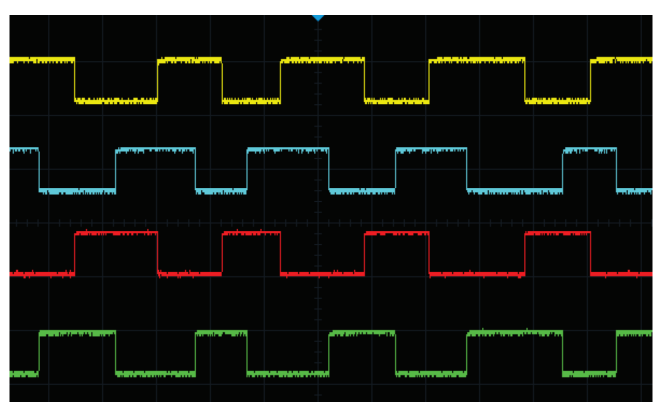

Figure 13 Square wave signal after converting

This square wave signal can be utilized for precision measurement purposes, allowing for the determination of the current displacement of the moving stage by the counting values. Additionally, this signal can serve as a laser encoder, providing feedback to the drive controller for feedback control. The integration of this signal as a laser encoder enhances the accuracy and reliability of feedback control systems, contributing to the overall advancement and competitiveness of industrial processes.

5 CONCLUSION

In this study, the optimization of interferometric system based on Fabry-Perot interferometer for advancing nanopositioning technologies in precision mechanical industries. This study has focused on developing a common-path structured interferometric system to eliminate DC offset, thereby enabling precise positioning control in normal environments. Furthermore, the utilization of polarizing phase-shifted methods and differential Fabry-Perot interferometers addresses limitations in determining movement direction and reduces signal drift, thereby enhancing measurement accuracy. Experimental validation demonstrates the correspondence between actual interference signals and simulations, thus validating the effectiveness of the proposed methods. Through signal processing and interpolation techniques, the resolution of the differential signal is enhanced, offering improved precision in displacement measurement and feedback control. Overall, the integration of interferometric systems as a laser encoder enhances the capabilities and reliability of nanopositioning systems, contributing to advancements in industrial processes and competitiveness.

6 REFERENCES

[1] Stuerzebecher, L., Fuchs, F., Zeitner, U. D. & Tuennermann, A. (2015). High-resolution proximity lithography for nano-optical components. *Microelectronic Engineering, 132*, 120-134. https://doi.org/10.1016/j.mee.2014.10.010

[2] Jaeger, G. (2010). Limitation of precision length measurements based on interfermeters. *Measurement*, *43*(5), 652-658. https://doi.org/10.1016/j.measurement.2009.12.030

[3] Chang, C. P., Tung, P. C., Shyu, L. H., Wang, Y. C., & Manske, E. (2013). Modified Fabry-Perot interferometer for displacement measurement in ultra large measuring range. *Review of Scientific Instruments*, *84*(5). https://doi.org/10.1063/1.4803672

[4] Chang, S. C., Chang, C. P., Wang, Y. C. & You, Z. F. (2022). Linear Displacement and Straightness Measurement by Fabry-Perot Interferometer Integrated with an Optoelectronic Module. *Tehnički glasnik, 16*(3), 420-425. https://doi.org/10.31803/tg-20220424124800

[5] Shyu, L. H., Chang, C. P. & Wang, Y. C. (2011). Influence of Intensity Loss in the Cavity of a Folded Fabry-Perot Interferometer on Interferometric Signals. *Review of Scientific instrument, 82*(6), 063103. https://doi.org/10.1063/1.3596451

[6] Chang, C. P., Tu, T. C., Huang, S. R., Wang, Y. C. & Chang, S. C. (2021). Development of the Heterodyne Laser Encoder System for the X-Y Positioning stage. *Sensors, 21*(17), 5775. https://doi.org/10.3390/s21175775

[7] Fabry, C. (1899). Theorie et applications d'une nouvelle methods de spectroscopie intereferentielle. *Ann. Chim. Ser. 7(16)*, 115-144.

[8] Lawall, J. R. (2005). Fabry–Perot metrology for displacements up to 50 mm. *JOSA A*, *22*(12), 2786-2798. https://doi.org/10.1364/JOSAA.22.002786

[9] Chang, C. P., Tung, P. C., Shyu, L. H., Wang, Y. C., & Manske, E. (2013). Multi-interferometric displacement measurement system with variable measurement mirrors. *Applied Optics*, *52*(17), 3902-3909. https://doi.org/10.1364/AO.52.003902

[10] Chang, C. P., Shih, Y. C., Chang, S. C. & Wang, Y. C. (2019). Laser encoder system for XY positioning stage. *Mechatronics*, *63*, 102274. https://doi.org/10.1016/j.mechatronics.2019.102274

[11] iC Haus Interpolation Products (2017, October 19, p. 15), online resource. Available from: https://www.ichaus.de/wp-content/uploads/TW8_datasheet_D3en.pdf

Authors' contacts:

Syuan-Cheng Chang, Assistant Professor
National Yunlin University of Science and Technology,
123 University Road, Section 3, Douliou, Yunlin 64002, Taiwan
tso1147279@gmail.com

Chung-Ping Chang, Associate Professor
(Corresponding author)
National Chiayi University,
300 Syuefu Road, Chiayi 600355, Taiwan
cpchang@mail.ncyu.edu.tw

Yung-Cheng Wang, Professor
National Yunlin University of Science and Technology,
123 University Road, Section 3, Douliou, Yunlin 64002, Taiwan
wangyc@yuntech.edu.tw